This article was downloaded by:
On: *25 January 2011*
Access details: *Access Details: Free Access*
Publisher *Taylor & Francis*
Informa Ltd Registered in England and Wales Registered Number: 1072954 Registered office: Mortimer House, 37-41 Mortimer Street, London W1T 3JH, UK

Liquid Crystals
Publication details, including instructions for authors and subscription information:
http://www.informaworld.com/smpp/title~content=t713926090

The stability of columns comprising alternating triphenylene and hexaphenyltriphenylene molecules: variations in the structure of the hexaphenyltriphenylene component

Richard J. Bushby[a]; Julie Fisher[b]; Owen R. Lozman[a]; Stephan Lange[a]; John E. Lydon[c]; Sholto R. McLaren[a]
[a] Centre for Self-Organising Molecular Systems (SOMS), University of Leeds, Leeds LS2 9JT, UK [b] School of Chemistry, University of Leeds, LEEDS LS2 9JT, UK [c] Department of Biochemistry and Molecular Biology, University of Leeds, Leeds LS2 9JT, UK

To cite this Article Bushby, Richard J. , Fisher, Julie , Lozman, Owen R. , Lange, Stephan , Lydon, John E. and McLaren, Sholto R.(2006) 'The stability of columns comprising alternating triphenylene and hexaphenyltriphenylene molecules: variations in the structure of the hexaphenyltriphenylene component', Liquid Crystals, 33: 6, 653 — 664
To link to this Article: DOI: 10.1080/02678290600682078
URL: http://dx.doi.org/10.1080/02678290600682078

PLEASE SCROLL DOWN FOR ARTICLE

Full terms and conditions of use: http://www.informaworld.com/terms-and-conditions-of-access.pdf

This article may be used for research, teaching and private study purposes. Any substantial or systematic reproduction, re-distribution, re-selling, loan or sub-licensing, systematic supply or distribution in any form to anyone is expressly forbidden.

The publisher does not give any warranty express or implied or make any representation that the contents will be complete or accurate or up to date. The accuracy of any instructions, formulae and drug doses should be independently verified with primary sources. The publisher shall not be liable for any loss, actions, claims, proceedings, demand or costs or damages whatsoever or howsoever caused arising directly or indirectly in connection with or arising out of the use of this material.

Liquid Crystals, Vol. 33, No. 6, June 2006, 653–664

Taylor & Francis
Taylor & Francis Group

The stability of columns comprising alternating triphenylene and hexaphenyltriphenylene molecules: variations in the structure of the hexaphenyltriphenylene component

RICHARD J. BUSHBY*†, JULIE FISHER‡, OWEN R. LOZMAN†, STEPHAN LANGE†, JOHN E. LYDON§ and SHOLTO R. MCLAREN†

†Centre for Self-Organising Molecular Systems (SOMS), University of Leeds, Woodhouse Lane, Leeds LS2 9JT, UK
‡School of Chemistry, University of Leeds, Woodhouse Lane, LEEDS LS2 9JT, UK
§Department of Biochemistry and Molecular Biology, University of Leeds, Woodhouse Lane, Leeds LS2 9JT, UK

(*Received 11 October 2005; in final form 26 January 2006; accepted 26 January 2006*)

Previous investigations of complementary polytopic interaction (CPI) columnar mesophases, in which the columns are built up of alternating hexaalkoxytriphenylene (HAT) and hexaphenyltriphenylene (PTP) molecules, concentrated mainly on the effect of variations in the structure of the HAT component. This investigation is concerned with the effect of variations in the structure of the PTP component and, in particular, variations in the position of an alkoxy side chain in the phenyl ring. Stable columnar mesophases are obtained when a hexyloxy substituent is placed in the *meta*- or *para*-position but not in the *ortho*-position. In the case of the *meta*- and *para*-substituted systems, the two-component CPI columnar phases are stable over a considerably larger temperature range than the one-component HAT systems. The evidence suggests that unfavourable PTP/PTP stacking is as much a driving force for the formation of these mixed stacks as is favourable PTP/HAT stacking, but both need to be explained in terms of the sum of atomically dispersed van der Waals and coulombic interactions. On cooling from the isotropic into the Col_h phase, the columnar phase based on a 1:1 mixture of hexakis(hexyloxy)tripenylene and the *meta*-hexyloxy-substituted PTP gives an unusual texture consisting of 'viking-axe'-shaped structures.

Downloaded At: 16:00 25 January 2011

1. Introduction

The stability of the Col_h phase of 2,3,6,7,10,11-hexakis(hexyloxy)triphenylene **1a** (HAT6) is substantially enhanced by adding one mole of 2,3,6,7,10,11-hexakis(4′-nonylphenyl)triphenylene **2a** (PTP9) (scheme 1) [1]. The columns in the resultant Col_h phase are built up from alternating HAT6 and PTP9 molecules as shown schematically in figure 1. The columns are highly ordered, and consequently charge-carrier mobilities along the column are high [2]. The origin of the high stability of this and related mixed columnar structures is intriguing. It does not appear to be the result of a charge-transfer interaction since the IR and UV spectra of the mixture are essentially the sum of those of the individual components, indicating that the electronic structures of the individual components are not perturbed [1]. Neither can a net molecular quadrupole interaction be invoked since, in some of the stabilized systems, the net quadrupole moments of the HAT and PTP components are the same, whereas in others they are opposite. So far, our best understanding as to the origin of their stability is provided by extended electron distribution (XED) force field calculations [3]. Since these employ quadrupolar and van der Waals terms calculated on an atom-by-atom basis, we have coined the term 'complementary polytopic interaction' (CPI) to describe the situation.

We have previously tested the predictive power of the XED programme to explain the effect of varying the structure of the HAT component. It was found that the formation of stable CPI HAT/PTP mixtures is not particularly sensitive to changes in the length and nature of the HAT peripheral alkyl chain, but that their formation can be disrupted by bulky substituents in the α-position of the triphenylene nucleus [4]. This paper is concerned with variations in the structure of the PTP component and, in particular, the difference in CPI-forming properties of molecules with peripheral hexyloxy groups in the *ortho*-, *meta*- and *para*-positions of the phenyl ring (scheme 2). The XED program predicts that the *meta*- and *para*-systems should form stable CPI

*Corresponding author. Email: R.J.Bushby@leeds.ac.uk

Liquid Crystals
ISSN 0267-8292 print/ISSN 1366-5855 online © 2006 Taylor & Francis
http://www.tandf.co.uk/journals
DOI: 10.1080/02678290600682078

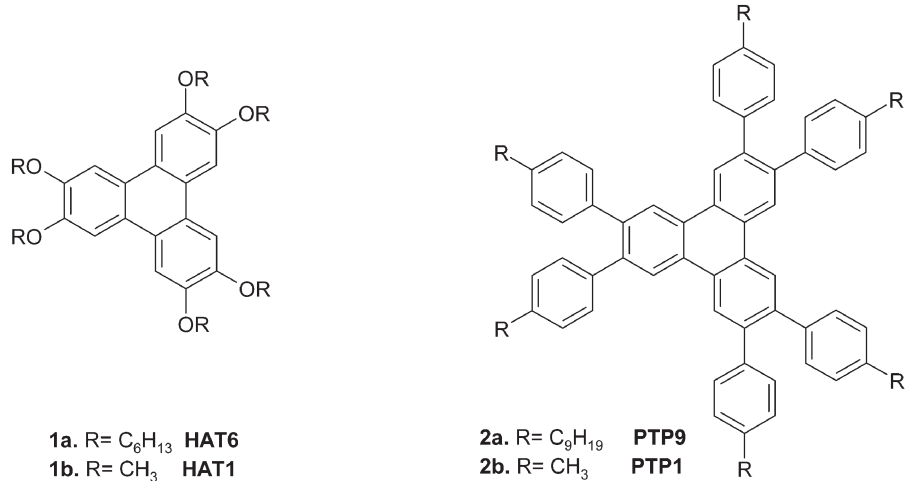

Scheme 1. Formulae of HAT **1a** and PTP **2a** compounds that form CPI columnar mesophases and the equivalent structures used for the molecular modelling, **1b** and **2b**.

systems but the *ortho*-isomer should not. Once again, these predictions proved to be correct.

The study also provides further general insights into the reasons for formation of CPI columnar phases over such extended temperature ranges. It suggests that the instability of single component PTP–PTP stacks is as much a driving force as is the stability of mixed PTP–HAT stacks.

2. Results and discussion

2.1. *Synthesis*

The synthesis of the *ortho*- *meta*- and *para*-isomers of 2,3,6,7,10,11-hexakis(hexyloxyphenyl)triphenylene **6a**–**c** followed the route shown in scheme 2. As in previous work, the Suzuki coupling reaction conditions had to be modified to avoid contamination with small amounts of penta-aryltriphenylenes, which otherwise arise from a side reaction in which there is reduction of the aryl bromide [5]. Under 'standard' Suzuki coupling conditions this only occurs at 1–2% per site, but since there are six sites of substitution per molecule substantial contamination with the penta-aryl product can occur and the byproduct is all but impossible to remove. The bromophenols **3a**–**c** were alkylated to give 2-, 3- and 4-hexyloxybromobenzene **4a**–**c**. These were treated with butyl lithium at −78°C, quenched with triisopropyl borate at −78°C and the reaction mixture stirred over night. HCl work-up yielded the boronic acids which were converted to the more stable pinacol esters **5a**–**c** by heating under reflux with pinacol and 3 Å molecular sieves in THF. The pinacol esters of the boronic acids were coupled with hexabromotriphenylene in the presence of barium hydroxide, water and tetrakistriphenylphosphinepalladium(0) in 1,2-dimethoxyethane (DME) to give the *ortho*-, *meta*- and *para*-isomers of 2,3,6,7,10,11-hexakis(hexyloxyphenyl)triphenylene (*o*-PTP06 **6a**, *m*-PTPO6 **6b** and *p*-PTP06 **6c**).

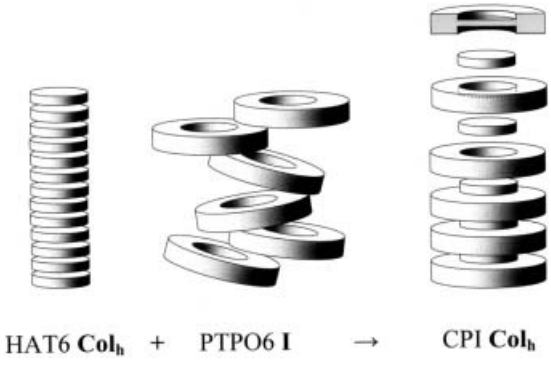

Figure 1. Schematic representation of the intercalation of PTP9 into columns of HAT6. The HAT molecules fit into the 'hollow' in the face of the PTP.

The ^{1}H NMR spectrum of *o*-PTPO6 **6a** contains more resonances than expected. Hence, as shown in figure 2, the signal for the –OCH_2CH_2– methylene protons showed at least four distinct multiplets rather than the expected triplet. This occurs because rotation about the triphenylene–phenyl bond is slow on the NMR timescale so that each rotomer gives a discrete spectrum. As shown in figure 2, on increasing the temperature to 100°C, the signals broaden but rotation does not become sufficiently rapid for the signals to coalesce. That there really is an equilibrium between various rotomers, was established by the saturation transfer (transfer of non-equilibrium spin) experiment shown in figure 3 [6]. In this, the sample is irradiated at the resonant frequency of a proton which undergoes exchange. The resultant difference spectrum shows a

Downloaded At: 16:00 25 January 2011

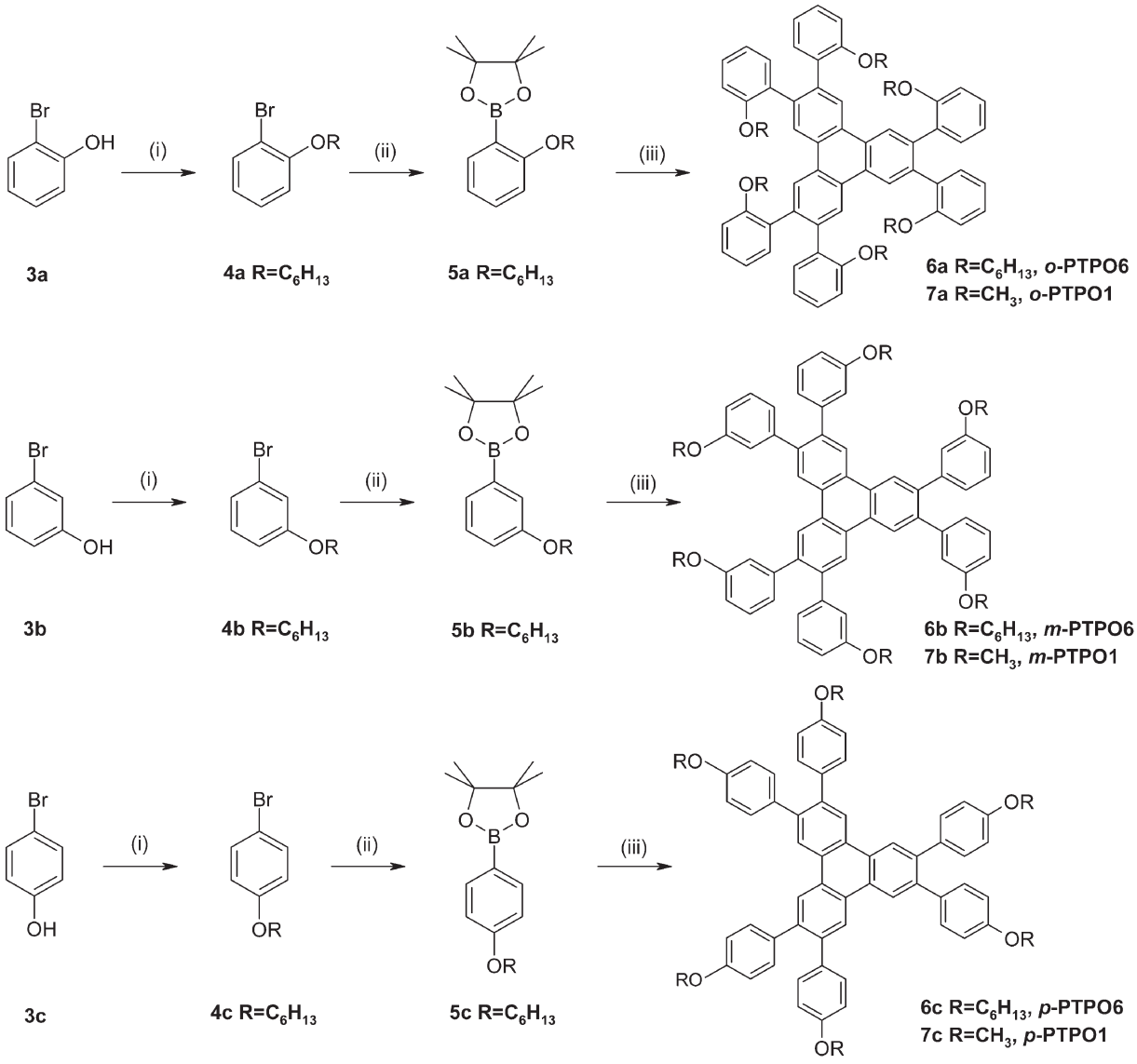

Scheme 2. Synthesis of *o*-PTP06 **6a**, *m*-PTP06 **6b** and *p*-PTP06 **6c**. (i) $C_6H_{13}Br/K_2CO_3/EtOH/reflux$. (ii) 1. BuLi/THF/−78°C; 2. $B(O^iPr)_3$/THF/−78°C; 3. 1M HCl; 4. Pinacol/THF/3 Å molecular sieve. (iii) Hexabromotriphenylene (1/7 eq.)/$Pd(PPh_3)_3$ (3 mol% per site)/$Ba(OH)_2/H_2O$/DME. **a**=*ortho*, **b**=*meta*, **c**=*para*.

large peak for the irradiated proton, along with smaller peaks for the protons that are thermally exchangeable with the irradiated proton (in-phase, direct transfer of non-equilibrium spin) and nOe coupled (out of phase). Sequential irradiation of the $-OCH_2CH_2-$ methylene protons (1–3) shows that they are all able to exchange with one other, confirming that all arise from rotomers, rather than distinct chemical entities.

2.2. *Molecular modelling*

The formation/non-formation of HAT/PTP pairs has previously been rationalized using the XED model [7], which so far this has proved to be the only reliable predictive tool [3]. In this model the π-stacking interaction is expressed as a sum of atom-centred van der Waals and coulombic (pole+dipole+quadrupole) terms. As in previous studies, the short chain analogues (PTPO1 **7a–c** and HAT1 **1b**, schemes 1 and 2) of the synthesized compounds were used to reduce computation time. The geometries of the molecules of interest were first optimized at the PM3 level and partial atomic charges were assigned. The addition of the extended electron distribution was followed by an exhaustive conformational search to find the 'true' global minimum geometry for each of the structures. From these optimized geometries a series of molecular docking

Downloaded At: 16:00 25 January 2011

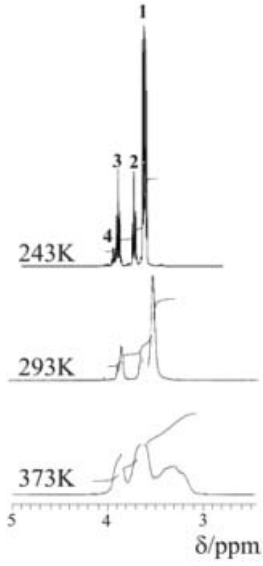

Figure 2. Changes in the ^{1}H NMR signal for the –OCH_2CH_2– methylene protons of *o*-PTP06 **6a** as a function of temperature in (CCl_2D_2).

Downloaded At: 16:00 25 January 2011

experiments were performed, where one molecule (the bullet) is docked to a spatially fixed second molecule (the target). Within the programme, the 'bullet' is 'fired' starting from a total of two hundred and fifty points around the surface of a sphere centred on the 'target'. In cases where there is a strongly preferred structure the same result is obtained many times but in any case the most stable pair can be found. Values for the overall energy of the docked pairs, as well as the coulombic and the van der Waals contributions to the interaction energies, are obtained. The total energies U_{AA} for forming the homo-dimers **1b**+**1b**, **7a**+**7a**, **7b**+**7b** and **7c**+**7c** are compared with the energies U_{AB} for the hetero-dimers **1b**+**7a**, **1b**+**7b** and **1b**+**7c**, The mixed dimers should be preferred if ΔE is negative in the equation:

$$\Delta E = U_{AB} - (U_{AA} + U_{BB})/2.$$

The results of the docking simulations for HAT1 **1b** and the PTPO1 isomers **7a**–**c** are shown in tables 1 and 2. The formation of stable hetero-dimers and hence of CPI 'compounds' is predicted to be favoured for the mixtures **1b**+**7b** and **1b**+**7c**, but not for **1b**+**7a**. Coulombic attraction is the main force stabilizing the CPI pair formed with the *meta*-isomer, whereas the van der Waals term makes the greatest contribution to stabilizing the CPI pair formed with the *para*-isomer. The geometries of the heterodimers are shown in figure 4. It is clear that there is a strong preference for the formation of linear AB stacks in the cases of *m*-PTPO1 **7b** and *p*-PTPO1 **7c** with HAT1 **1b**. It is equally evident that the packing in the *o*-PTPO1 **7a** mixture with HAT1 **1b** is very different. In this case the steric congestion around the phenyl–triphenylene ring prevents the two aromatic nuclei from achieving such a close approach and this destabilizes the mixed dimer.

2.3. *Phase behaviour*

DSC data for the materials studied is summarized in table 3. None of the products **6a**–**c** are themselves mesogenic, but *m*-PTPO6 **6b** and *p*-PTPO6 **6c** both form stable liquid crystalline CPI 'compounds' with HAT6 **1a**, giving Col_h phases in the ranges 25–111°C and 25–196°C respectively (table 1). *o*-PTPO6 **2a** does not form a homogeneous mixture with HAT6 **1a**.

The temperature/composition phase diagram for the HAT6/*p*-PTPO6 system seems to be similar to that for the HAT6/PTP9 system which we have previously studied in more detail [8, 9]. Hence, based on more limited experimental data, a phase diagram for the HAT6/*p*-PTPO6 is sketched in figure 5. The experimental points (obtained from both optical microsocopy and DSC) are indicated and phase boundaries have been drawn using the same principles as for HAT6/PTP9. The more speculative features are indicated by broken lines. As for HAT6/PTP9, the maximum in the clearing curve indicates 'compound' formation (in the phase diagram sense of the word) and, as expected for an alternating A/B structure, the CPI 'compound' is formed at an exact 1:1 molar ratio. It gives a columnar discotic phase from below room temperature up to its clearing point of 196°C. As found in the study of HAT6/PTP9, this phase is remarkably limited in its ability to accept an excess of either the PTP or the HAT component and the region of the phase diagram which it occupies is a narrow vertical band. We have found it difficult to identify the precise positions of the vertical boundaries of this band but we judge that they can be no more than 1% to the right and left of the central 50% line. This lack of misciblity means that the phase diagram is dominated by large, symmetrically disposed, two-phase regions. The curve drawn for the liquidus was calculated on the assumption of ideal behaviour of the two components [8, 9] but it fits reasonably well to the experimental points. This seems to imply that, within the isotropic liquid, the associated columnar structure does not persist and that it disintegrates when the CPI Col_h phase disappears. Hence, there is a synergism whereby the order within the mesophase also contributes to the stability of the structure. We visualize this synergism as breaking down catastrophically at the clearing point when the columns fall apart and the mesophase melts to give the isotropic liquid.

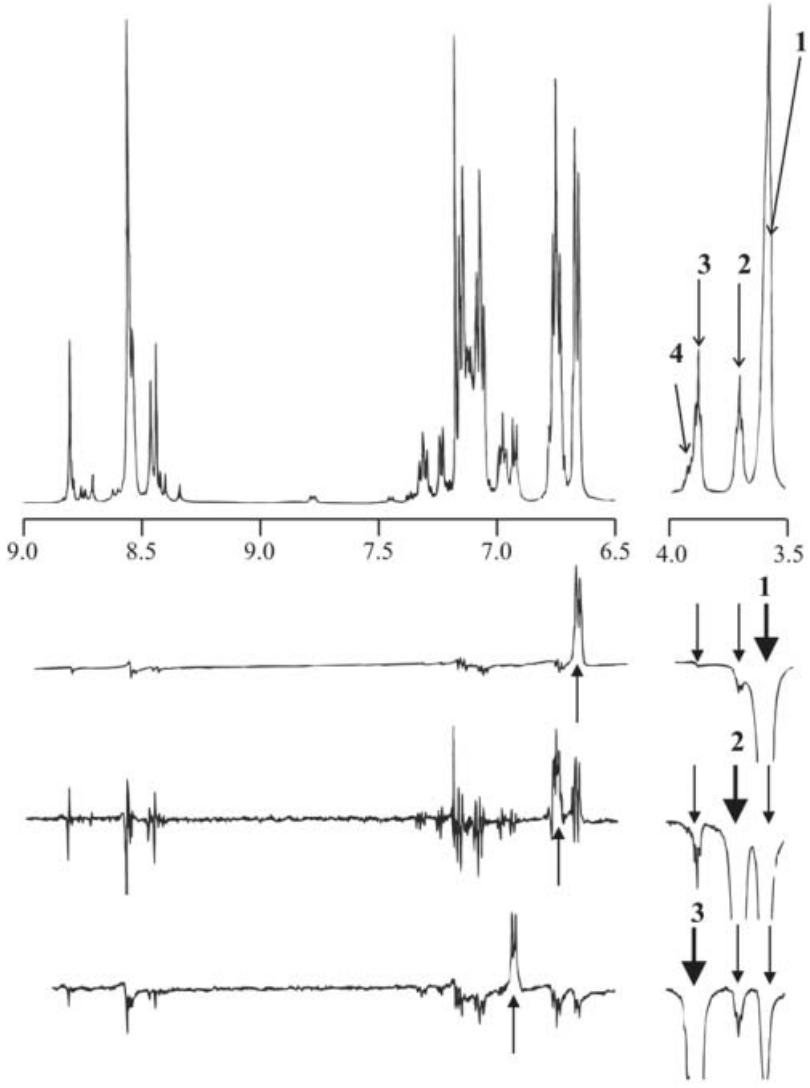

Figure 3. The top line shows the aromatic and Tp-OCH_2 methylene protons (labelled in order 1–4) from the ^{1}H NMR spectrum of *o*-PTP06 **6a** in $CDCl_3$ at room temperature. The lines below show the results of the saturation transfer experiments in which protons 1, 2 and 3 are irradiated ($\downarrow$). In-phase saturation transfer, indicating chemical exchange, occurs to the protons labelled $\downarrow$. Out of phase nOe is observed between the saturated proton resonance and those labelled $\uparrow$.

Table 4 lists the powder X-ray diffraction results obtained for the columnar mesophases of the CPI 'compounds' HAT6+*m*-PTP and HAT 6+*p*-PTP. In the Col_h phase, HAT 6 gives a strong, moderately sharp 3.5 Å reflection (corresponding to the stacking repeat along the columns), two reflections in a ratio of $1:1/\sqrt{3}$ characteristic of the hexagonal lattice, and a diffuse 4 Å peak, arising from the disordered alkyl chains. The CPI columnar phases give many more reflections than HAT but the reflections can still be indexed in terms of a two-dimensional hexagonal cell (table 4). The patterns are indexable in terms of *h k* 0 and 0 0 1 reflections, and other than a possible but ambiguous assignment of '1 0 1?' (which may be indicative of a plastic columnar phase [10]) there is no need to invoke reflections of the general *h k l* type. The increased number of reflections in the CPI 'compounds' could arise from the differences in the 'molecular' transform of the columns (with the structure having more 'contrast' for X-rays and hence larger structure factors), but a more likely explanation is that there is an increase in the range of the lateral ordering. In the proposed $(AB)_n$ stacking of the molecules the repeat distance along the column axis has doubled so there should be an axial reflection at 7 Å (together with its second order at 3.5 Å). This is observed in the *o*-PTP but not the *m*-PTP system. However, this does not necessarily imply any difference in structure of the two CPI phases. The central cores of

Downloaded At: 16:00 25 January 2011

Table 1. XED molecular docking energies for homo-dimers U_{AA} and heterodimers U_{AB}, including coulombic and van der Waals contributions. All energies are in kcal mol^{-1}.

Molecule 1	Molecule 2	E_{total}	$E_{coulomb}$	E_{vdw}
HAT 1 **1b**	HAT 1 **1b**	−39.8	−2.5	−37.3
o-PTPO1 **7a**	*o*-PTPO1 **7a**	−51.6	−4.8	−46.8
m-PTPO1 **7b**	*m*-PTPO1 **7b**	−42.5	+3.3	−45.8
p-PTPO1 **7c**	*p*-PTPO1 **7c**	−45.0	−7.8	−37.2
PTP2O1 **8b**	PTP2O1 **8b**	−41.0[a]	+2.1[a]	−43.1[a]
*x*PTP2O1 **9b**	*x* PTP2O1 **9b**	−91.2[a]	−7.3[a]	−83.9[a]
HAT1 **1b**	*o*-PTPO1 **7a**	−33.9	+1.3	−35.2
HAT1 **1b**	*m*-PTPO1 **7b**	−49.7	−6.0	−43.6
HAT1 **1b**	*p*-PTPO1 **7c**	−50.5	−6.5	−44.1
HAT1 **1b**	PTP2O1 **8b**	−32.6[a]	−4.6[a]	−28.0[a]
HAT1 **1b**	*x* PTP2O1 **9b**	−34.5[a]	+0.4[a]	−34.9[a]

[a]Ref. [3].

Table 2. Values of $\Delta E = U_{AB} - \frac{1}{2}(U_{AA}+U_{BB})$. A CPI 'compound' is predicted to form if the mixed dimer is more stable than the two isolated dimers, i.e. if ΔE is negative. All energies are in kcal mol^{-1}.

System	ΔE_{total}	$\Delta E_{coulomb}$	ΔE_{vdw}	CPI predicted	CPI observed
o-PTPO1	+11.8	+5.0	+6.9	No	No
m-PTPO1	−8.5	−6.4	−2.1	Yes	Yes
p-PTPO1	−8.1	−1.4	−6.9	Yes	Yes
PTP2O1	+7.8[a]	−4.4	+11.2	No	No
*x*PTP2O1	+31.0[a]	+5.3	+25.7	No	No

[a]Ref. [3].

Downloaded At: 16:00 25 January 2011

HAT and PTP are similar and the peripheral groups are fairly mobile. Hence, the whole column may well appear to be a stack of near-identical molecules. If (for example) these were arranged in a $\sim 2_1$ screw axis there would be a systematic absence for the 0 0 1, 7 Å reflection and the first axial reflection would be the 0 0 2 at 3.5 Å.

The optical texture of *p*-PTPO6+HAT6 viewed through crossed polarizers is typical of that seen for many other Col_h systems. However, the optical texture for the Col_h phase of *m*-PTPO6+HAT6 is unusual. It shows curved dendritic growths which often start as symmetrical 'viking axe' structures as shown in figure 6. Whilst we have not peviously encountered this in mesogenic materials we are grateful to Prof. G. Ungar [11] who has pointed out that this morphology is not uncommon in a range of other soft materials but particularly in polymers [12]. It is associated with branching/dendritic growth [13].

3. Conclusions

Once again [3, 14, 15] we have found that the XED force field is remarkably successful in predicting whether or not stable CPI columnar phases will be formed and hence that the basic approach of treating the π-stacking interaction, in terms of the sum of many dispersed van der Waals and coulombic terms, is probably correct. As shown in figure 4 and in previous work [3], the programme predicts that, within the stack, the HAT molecule fits neatly into the 'hollow' in the surface of the PTP molecule created by the canting of the peripheral phenyl rings. In figures 1 and 7 we have tried to represent the relationship between the two molecules schematically by showing the PTP as a disk with a HAT-sized 'hollow' in each face. This schematic representation clarifies both of the two main driving forces behind the formation of CPI columnar systems: the good fit between HAT and PTP, and the poor fit of the PTP to itself.

The first significant factor is the good fit of the HAT into the hollow in the face of the PTP. In this paper we show that this can be disrupted by bulky *ortho*-substituents on the phenyl rings of the PTP nucleus and we have previously shown that it can also be disrupted by bulky α-substituents on the triphenylene nucleus of the HAT [3]. In this respect, note the predicted non-parallel stacking of HAT1 and *o*-PTP1 as compared with the parallel stacking HAT1 and *m*-PTP1 or HAT1 and *p*-PTP1 in figure 4. Note also in table 1 the resultant lower attractive interaction, particularly the lower van der Waals interaction, between HAT1 and *o*-PTP1 as compared with HAT1 and *m*-PTP1 or

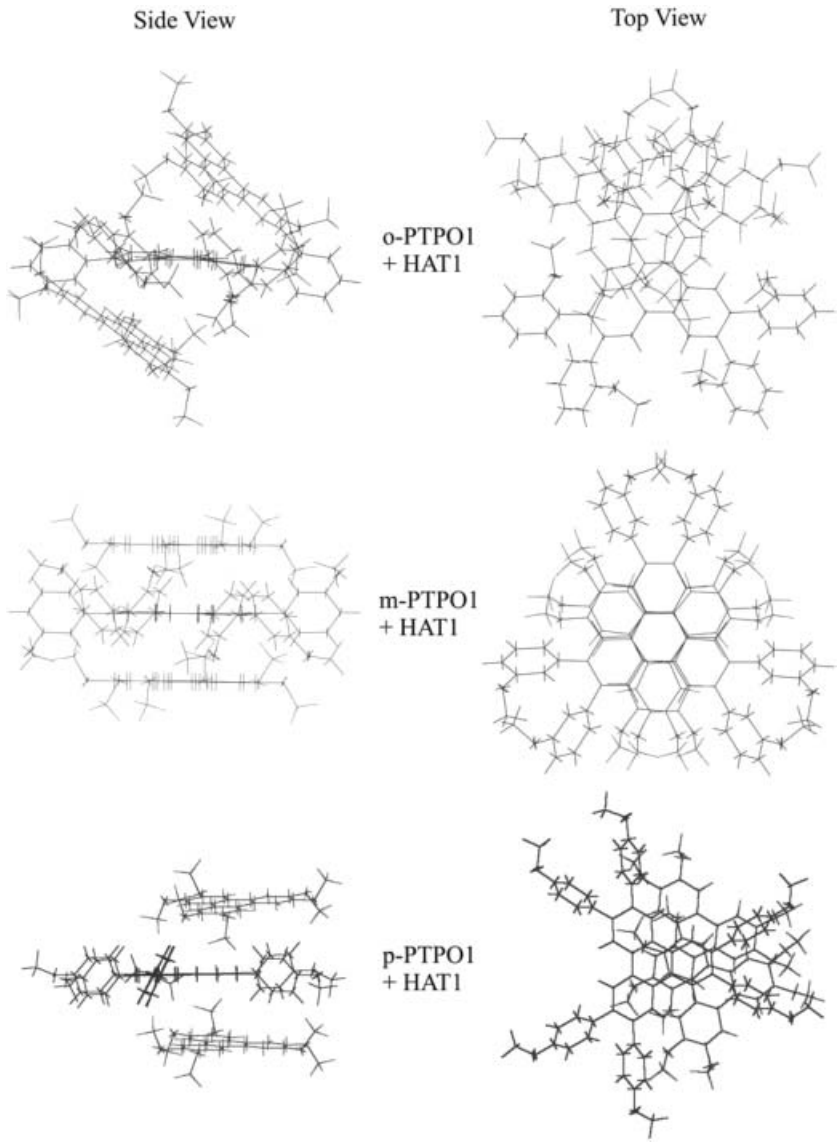

Figure 4. Side and top views of the XED minimum energy geometries for hetero-dimers of HAT1 with isomers of PTPO1. In each case the central PTP was the 'stationary target' and the HAT molecule the 'mobile bullet'. Two equivalent minimum energy positions were detected for the HAT1 : one above and one below the PTP. Both are shown.

HAT1 and *p*-PTP1. Further, it seems that complementary stacking of HAT and PTP is a specific feature of the columnar structure. Hence, in the phase diagram (figure 5), there is a wide two-phase region, but the clearing point curve is almost flat over the central composition range. Whereas the columnar phase is stable over only a very small composition range (its stability is linked to an exact alternating structure), the isotropic liquid shows almost ideal behaviour in which the two molecular components behave essentially independently over a wide composition range.

The second important factor in the formation of these CPI columnar systems is the poor fit of the PTP to itself. The canted peripheral phenyl rings make it impossible to bring the whole of the two π-systems together. In table 1, the self-stacking of a non-planar PTP, PTP2O1 **8b** (figure 7), is compared with the self-stacking of the equivalent, almost planar molecule *x*PTP2O1. The difference in geometry results in a dramatic difference between the homo-dimerization energies and particularly the van der Waals component of the homo-dimerization energies. Indeed, as compared with *x*PTP2O1, all of the PTP systems listed in table 1 can be see to have low homo-dimerization energies. The shape of PTP makes it impossible to bring large areas of the surface together in the manner that would lead to a

Downloaded At: 16:00 25 January 2011

Table 3. DSC data; all values are from the second heating cycle, except where stated.

Material	Phase behaviour/°C (J g^{-1})
HAT6 **1a**	Cr 70 (48) Col_h 100 (6) I
o-PTPO6 **6a**	Cr_1 28.0 (1.3) Cr_2 81.4 (17.7)[a] I
o-PTPO6 **6a**+HAT6 **1a**	Cr 68.0 (14.9)[b] I
m-PTPO6 **6b**	Cr 11.4 (1.7) I[c]
m-PTPO6 **6b**+HAT6 **1a**	Col_h 111.0 (26.1) I
p-PTPO6 **6c**	Glass 103.0 (−52.0) Cr_1 143.0 (4.0) Cr_2 156.0 (52.0) I
p-PTPO6 **6c**+HAT6 **1a**	Col_h 196.0°C (28.6)

[a]Cr_2 was detected only during the first heating cycle. [b]Values for first heating cycle; did not recrystallize from the melt. [c]Melting of partially crystallized material.

large van der Waals component in the attractive force. In this respect, PTP is analogous to the tryptycene systems of Swagger *et al.* [16, 17] and the spiro-fused indane polymers of McKeown *et al.* [18, 19]. As with PTP, it is the intrinsically poor self-stacking of tryptycene and of spirobisindane that facilitates the formation of stable structures in which smaller molecular species can fill the gaps.

Hence, the present study has also gone some way to clarifying the general reasons for the formation of the CPI Col_h phase between HAT and PTP. The formation of the CPI columnar system is seen as the result both of the good fit of HAT to PTP and of the poor fit of PTP to itself. As in other π-stacked systems, the molecular interactions at small separations are best represented as a sum of atom-centred van der Waals and coulombic terms [3, 14, 15]. In the specific case of HAT and PTP the marked stabilization of the columnar structure results in improved handling properties, mesophase ranges and charge-carrier mobilities and it is these factors that have the potential to lead to novel applications [20].

4. Experimental

4.1. *General procedures and instrumentation*

All chemicals and solvents were obtained from Sigma-Aldrich and were used without further purification. Routine nuclear magnetic resonance spectra were recorded on a Bruker DPX300 spectrometer. Chemical shifts are expressed in parts per million (ppm), relative to TMS. Mass spectra were recorded on a VG autospec spectrometer. FTIR spectra were recorded using a Perkin–Elmer 1760X FTIR spectrometer. DSC was performed on a Perkin–Elmer 7 thermal analysis system in closed aluminium pans at heating and cooling rates of 10°C min^{-1}. Optical polarizing microscopy was performed on an Olympus BH-2 microscope with a Linkam hot stage. Microanalyses were carried out at Leeds University Microanalytical Laboratory. X-ray diffraction experiments were performed using nickel filtered Cu K_α radiation (λ=0.154 nm). Column chro-

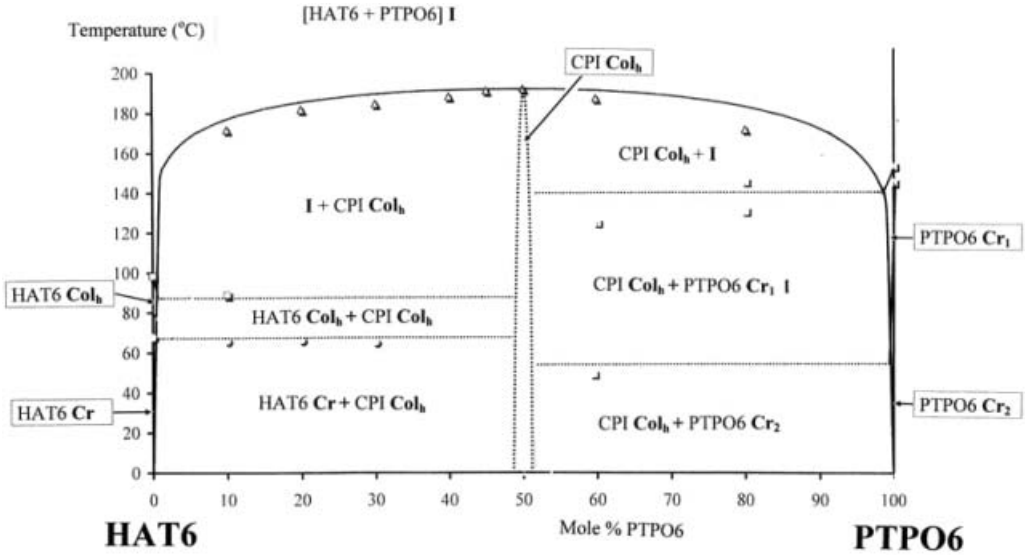

Figure 5. Phase diagram for the HAT6/*p*-PTPO6 system. The experimental clearing temperatures Δ are fitted to the equation $\ln 4x_A(1-x_A)=(2\Delta H_{AB}/R)(1/T_m-1/T)$ which assumes ideal behaviour in the liquid [8, 9]. Below the clearing point, phase separation occurs. The width of the CPI Col_h phase region is unknown but small. Below about 125°C the CPI Col_h phase becomes glassy and samples can no longer be sheared

Downloaded At: 16:00 25 January 2011

Table 4. Indexing of *d*-spacings (Å), determined by X-ray powder diffraction for the CPI 'compound' of *m*-PTPO6 **6b** and HAT6 **1a** and of *p*-PTPO6 **6c** and HAT6 **1a** (calculated values for a hexagonal unit cell with a=24.4 and c=3.6 Å).

	m-PTPO6 **6b** and HAT6 **1a**		*p*-PTPO6 **6c** and HAT6 **1a**		
h k l	30°C	100°C	30°C	130°C	Calculated for a=24.4 Å, c=3.6 Å
1 0 0[a]	20.5	21.2	20.2	21.2	21.1
1 1 0	—	—	12.4	12.4	12.7
2 0 0	10.9	10.1	10.7	—	10.5
2 1 0	—	—	8.0	8.2	8.0
0 0 ½	—	—	7.1	7.2	7.0
2 2 0	6.3	—	6. 3	6.5	6.1
4 0 0	5.3	—	5.4	5.4	5.3
Chain	4.1[b]	4.0[b]	4.1[b]	4.1[b]	~4[b]
0 0 1	3.6	—	3.6	3.7	3.6
1 0 1?	3.5	3.5	3.5	3.6	3.5

[a]1 0 $\bar{1}$ 0 indexed using the *h k i l* convention for a hexagonal lattice. [b]Diffuse.

matography was performed on Merck silica gel, thin layer chromatography on pre-coated aluminium-backed silica plates. Petroleum ether refers to the petroleum distillate fraction boiling at 40–60°C.

4.2. *Synthesis of hexyloxybromobenzenes (4)*

One equivalent of the desired bromophenol **3a**–**c**, 1.5 equiv of 1-bromohexane and 1.5 equiv of potassium carbonate were heated under reflux in dry ethanol under nitrogen. The reaction end was indicated by thin layer chromatography (DCM petroleum ether 1/1). The reaction mixture was filtered through celite, and the solvent removed *in vacuo*, giving an orange oil which was distilled at reduced pressure (0.1 mbar), yielding **4** as a colourless oil.

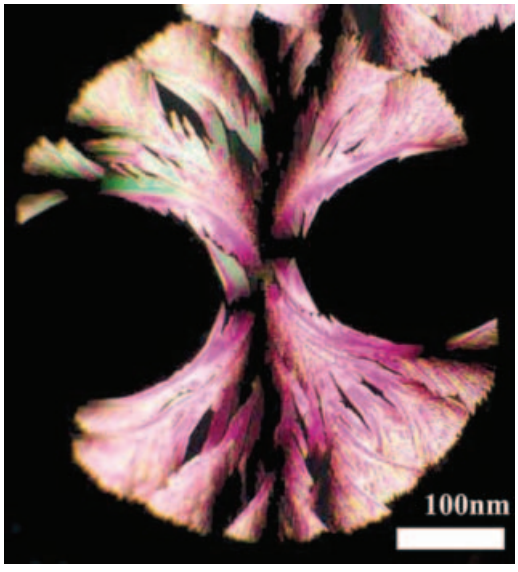

Figure 6. The 'viking axe' texture observed as the Col_h phase of *m*-PTPO6 **6b**+HAT6 **1a** grows from the isotopic liquid just below 111°C.

4.2.1. 2-Hexyloxybromobenzene (4a). Yield 92%, b.p. 118–120°C at *c*.0.1 mbar. ^{1}H NMR ($CDCl_3$) 7.54–7.51 (m, 1H, *H6*), 7.27–7.21 (m, 1H, *H4*), 6.89–6.78 (m, 2H, *H3* and *H5*), 4.01 (t, J=6.5 Hz, 2H, $ArOCH_2$), 1.83 (quintet, J=6.5 Hz, 2H, $ArOCH_2CH_2$), 1.55–1.45 (m, 2H, $ArOCH_2CH_2CH_2$), 1.42–1.32 (m, 4H, $ArO(CH_2)_3CH_2CH_2$), 0.91 (t, J=7.0 Hz, 3H, $ArO(CH_2)_5CH_3$). MS (EI, *m*/*z*) 257 (M^+, 10%), 173 (100%), 94.(10%), 63 (14%), 43 (78%). IR (liquid film, cm^{-1}) 2931 (C–H), 1587 (C=C, aromatic), 1467 (C=C, aromatic). Elemental analysis: found, C 55.8, H 6.4, Br 30.9; calc. for $C_{12}H_{17}BrO$, C 56.1, H 6.7, Br 31.1%.

4.2.2. 3-Hexyloxybromobenzene (4b). Yield 92%, b.p. 114°C at *c*.0.1 mbar. ^{1}H NMR ($CDCl_3$) 7.15–7.04 (m, 3H, *H2*,*H5*, and *H6*), 6.83–6.79 (m, 1H, *4H*), 3.91 (t, J=6.5 Hz, 2H, $ArOCH_2$), 1.76 (quintet, J=6.5 Hz, 2H, $ArOCH_2CH_2$), 1.49–1.39 (m, 2H, $ArOCH_2CH_2CH_2$), 1.38–1.28 (m, 4H, $ArO(CH_2)_3CH_2CH_2$), 0.90 (t, J=6.8 Hz, 3H, $ArO(CH_2)_5CH_3$). MS (FAB, *m*/*z*) 256 (M^+, 100%). IR (liquid film, cm^{-1}) 2931 (C–H), 1590 (C=C, aromatic). Elemental analysis: found, C 55.8, H 6.3%; calc. for $C_{12}H_{17}BrO$, C 56.1, H 6.7%.

4.2.3. 4-Hexyloxybromobenzene (4c). Yield 72%, b.p. 120–122°C at *c* 0.1 mbar. ^{1}H NMR ($CDCl_3$) 7.38–7.32 (m, 2H, *H2* and *H6*), 6.79–6.74 (m, 2H, *H3* and *H5*), 3.90 (t, J=6.6 Hz, 2H, $ArOCH_2$), 1.76 (quintet, J=6.6 Hz, 2H, $ArOCH_2CH_2$), 1.49–1.39 (m, 2H, $ArOCH_2CH_2CH_2$), 1.38–1.28 (m, 4H, $ArO(CH_2)_3CH_2CH_2$), 0.90 (t, J=6.8 Hz, 3H, $ArO(CH_2)_5CH_3$). MS (EI, *m*/*z*) 258 (M^+, 14%), 172 (100%), 143 (26%), 93 (12%), 63 (44%). IR (liquid film, cm^{-1}) 2931 (C–H), 1591 (C=C, aromatic), 1489 (C=C, aromatic).

Downloaded At: 16:00 25 January 2011

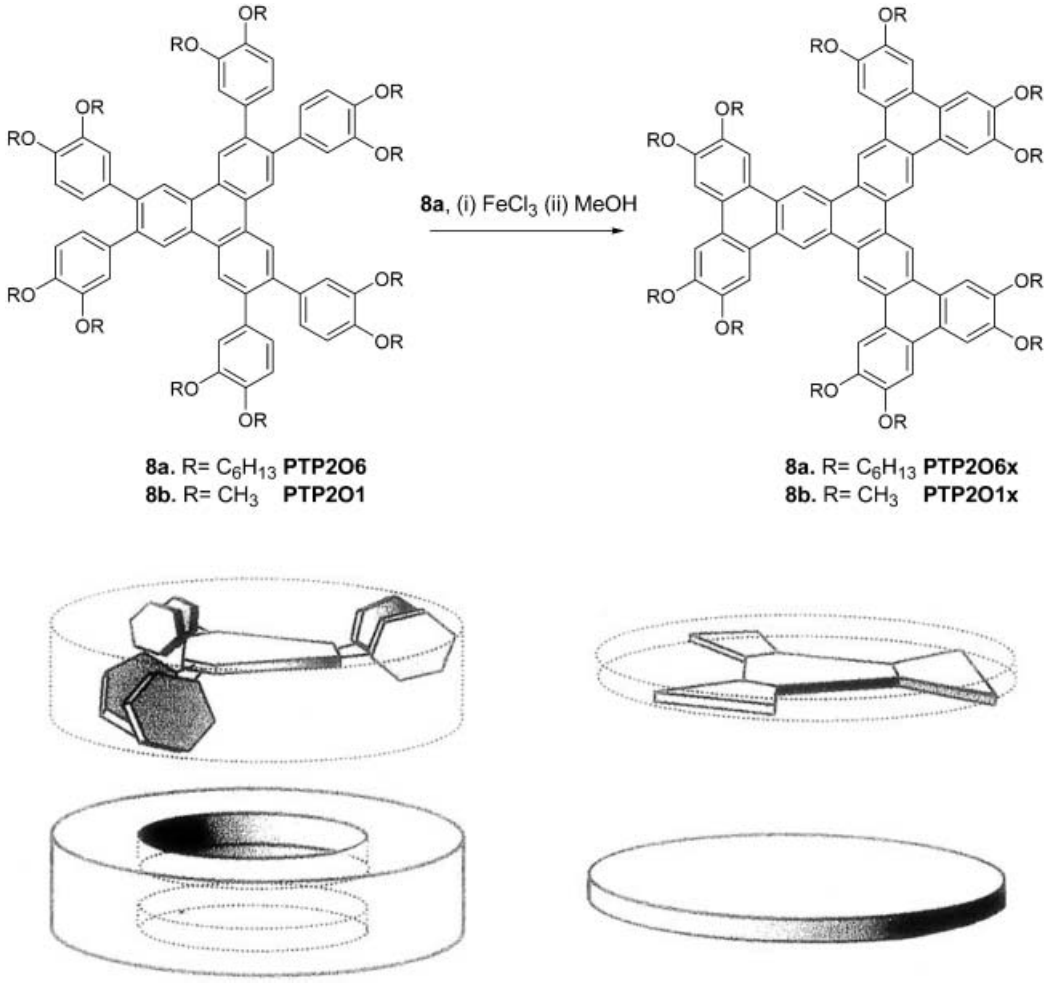

Figure 7. Formulae and schematic representations of PTP2O and *x*PTP2O systems **8** and **9**. The non-planar nature of the PTP leads to a much weaker van der Waals attractive interaction when two molecules are stacked one above the other.

Downloaded At: 16:00 25 January 2011

4.3. *Synthesis of pinacol esters of the hexyloxybenzene boronic acids (5)*

One equivalent of the required hexyloxybromobenzene **4** in 150 ml dry THF was cooled to −78°C under nitrogen. One equivalent of butyl lithium (2.5M in hexanes) was added dropwise at −78°C. Strirring was maintained for 3 h. The reaction was quenched through the dropwise addition of 1.1 equivalents of triisopropyl borate in 25 ml dry THF. The reaction mixture was then allowed to warm from −78°C to room temperature overnight prior to workup with 120 ml HCl (2M aqueous solution). After 1 h of stirring, the organic phase was separated and the aqueous phase extracted with diethyl ether (2 × 100 ml). The combined organic layers were, washed with water (2 × 100 ml), separated, dried with magnesium sulphate, filtered and stripped of solvent *in vacuo* without heating. The crude *ortho*-isomer was obtained as an orange liquid and purified by column chromatography on flash silica, with DCM/petroleum ether (8/2) eluant, yielding colourless crystals. For the *meta*- and *para*-isomers the crude boronic acids were obtained as slightly yellow crystals upon isolation from solvent and were used in the next step without further purification.

One equivalent of the desired hexyloxybenzene boronic acid and one equivalent of pinacol were heated under reflux overnight in dry THF containing 3 Å molecular sieves. The end point of the reaction was determined by thin layer chromatography (DCM/petroleum ether, 1/1 on silica). Upon cooling, the mixture was filtered through celite. Removal of the solvent *in vacuo* gave the crude product as a yellow oil. This was partially purified by column chromatography on flash silica, eluting with DCM/petroleum ether (1/4). The esters were isolated as colourless oils in quantitative yields and were used without further purification.

Downloaded At: 16:00 25 January 2011

4.3.1. Pinacol ester of 2-hexyloxybenzene boronic acid (5a). ^{1}H NMR ($CDCl_3$) 7.63–7.61 (m, 1H, ArH), 7.4–7.3 (m, 1H, ArH), 6.95–6.91 (m, 1H, ArH), 6.84–6.81 (m, 1H, ArH), 3.96 (t, J=6.2 Hz, 2H, $ArOCH_2$), 1.79 (quintet, J=6.5 Hz, 2H, $ArOCH_2CH_2$), 1.6–1.5 (m, 2H, $ArOCH_2CH_2CH_2$), 1.37–1.33 (m, 16H, $ArO(CH_2)_3CH_2CH_2$ and 4 × pinacol–CH_3), 0.91 (t, J=6.8 Hz, 3H, $ArO(CH_2)_5CH_3$). MS (EI, *m*/*z*) 304 (M^+, 20%), 163 (100%), 120 (19%), 83 (7%). IR (liquid film, cm^{-1}) 2930 (C–H), 1600 (C=C). Elemental analysis: found, C 70.6, H 9.7; calc. for $C_{18}H_{29}O_3B$, C 71.0, H 9.7%.

4.3.2. Pinacol ester of 3-hexyloxybenzene boronic acid (5b). ^{1}H NMR ($CDCl_3$) 7.39–7.26 (m, 3H, 3 × ArH), 7.02–6.98 (m, 1H, ArH), 3.98 (t, J=6.5 Hz, 2H, $ArOCH_2$), 1.77 (quintet, J=6.7 Hz, 2H, $ArOCH_2CH_2$), 1.5–1.4 (m, 2H, $ArOCH_2CH_2CH_2$), 1.34–1.25 (m, 16H, $ArO(CH_2)_3CH_2CH_2$ and 4 × pinacol-CH_3), 0.90 (t, J=6.8 Hz, 3H, $ArO(CH_2)_5CH_3$). MS (FAB, *m*/*z*) 304 (M^+, 100%), 161 (6%), 134 (29%), 101 (48%). IR (liquid film, cm^{-1}) 2931 (C–H).

4.3.3. Pinacol ester of 4-hexyloxybenzene boronic acid (5c). ^{1}H NMR 7.95–7.72 (m, 2H, 2 × ArH), 6.90–6.87 (m, 2H, 2 × ArH), 3.97 (t, J=6.6 Hz, 2H, $ArOCH_2$), 1.78 (quintet, J=6.9 Hz, 2H, $ArOCH_2CH_2$), 1.47–1.40 (m, 2H, $ArOCH_2CH_2CH_2$), 1.35–1.33 (m, 16H, $ArO(CH_2)_3CH_2CH_2$ and 4 × pinacol–CH_3), 0.90 (t, J=6.7 Hz, 3H, $ArO(CH_2)_5CH_3$). MS (FAB, *m*/*z*) 304 (M^+, 100%), 121 (8%), 101 (25%); IR (liquid film, cm^{-1}) 2932 (C–H), 1605 (C=C) Elemental analysis: found, C 70.9, H 9.7; calc. for $C_{18}H_{29}O_3B$, 71.0, H, 9.7%.

4.4. *Synthesis of 2,3,6,7,10,11-hexakis(hexyloxyphenyl)triphenylenes PTPO6 (6)*

Seven equivalents of the required pinacol ester of hexyloxybenzene boronic acid **5**, 1 equivalent of hexabromotriphenylene and 2 ml of water in dimethoxyethane (DME) were degassed with argon for 0.5 h. Seven equivalents of barium hydroxide monohydrate and tetrakistriphenylphosphinepalladium(0) (2.9 mol% per reaction site) were added under a stream of argon. The mixture was heated at 80°C under argon for seven days with stirring. The progress of the reaction was monitored by thin layer chromatography. Upon cooling to room temperature 2 ml of 30% H_2O_2 was added and the mixture stirred for 1 h. The mixture was filtered through celite, washed with water (5 × 100 ml) and stripped of solvent *in vacuo*. Crude products were obtained as yellow solids and purified by column chromatography on flash silica gel eluting with DCM/hexane (1/2) followed by recrystallization from ethanol. The *ortho*- and *para*-isomers were isolated as fine white crystals, the *meta*-isomer as a viscous, sticky oil, which gradually crystallized at room temperature.

4.4.1. *o*-PTPO6 (6a). Yield 57%, m.p. 81°C. ^{1}H NMR ($CDCl_3$) (figure 2) 8.5–8.7 (m, 6H, triphenyleneH), 7.24–7.12 (m, 12H, ArH), 6.87–6.71 (m, 12H, ArH), 3.5–3.7 (four t, J=6.2 Hz, 12H, 6 × $ArOCH_2$), 1.55 (m, 12H, $ArOCH_2CH_2$), 1.4–1.1 (m, 36H, $ArOCH_2CH_2CH_2CH_2CH_2$), 0.73 (m, 18H, $ArO(CH_2)_5CH_3$). ^{13}C NMR ($CDCl_3$) 156.0 (C, phenyl), 138.3 (C, phenyl), 137.5 (C, triphenylene), 132.4 (C, phenyl), 128.4 (C, phenyl), 127.9 (C, triphenylene), 125.8 (C, triphenylene), 120.0 (C, phenyl), 111.8 (C, phenyl), 67.9 (CH_2, sp^3), 31.5 (CH_2, sp^3), 28.9 (CH_2, sp^3), 25.5 (CH_2, sp^3), 22.4 (CH_2, sp^3), 13.9 (CH_3, sp^3). MS (FAB, *m*/*z*) 1284 (M^+, 100%), 1186 (13%), 1108 (14%), 1024 (6%), 865 (7%), 781 (29%), 688 (12%). IR (powder, cm^{-1}) 2915 (C–H), 1579 (C=C). Elemental analysis: found, C 83.8, H 8.7; calc. for $C_{90}H_{108}O_6$, C 84.1, H 8.5%.

4.4.2. *m*-PTPO6 (6b). Yield 66%, m.p. ~room temperature. ^{1}H NMR ($CDCl_3$) 8.71 (s, 6H, triphenyleneH), 7.24–7.19 (m, 6H, H5,), 6.95–6.93 (m, 6H, H6), 6.84–6.81 (m, 12H, H2 and H4), 3.79 (t, J=6.6 Hz, 12H, $ArOCH_2$), 1.69 (quintet, J=6.6 Hz, 12H, $ArOCH_2CH_2$), 1.45–1.20 (m, 36H, $ArOCH_2CH_2CH_2CH_2CH_2$), 0.90 (t, J=6.7 Hz, 18H, $ArO(CH_2)_5CH_3$). ^{13}C NMR ($CDCl_3$) 159.1 (C, phenyl), 143.1 (C, triphenylene), 140.3 (C, phenyl), 129.4 (C, triphenylene), 129.3 (C, triphenylene), 125.7 (C, phenyl), 122.7 (C, phenyl), 116.3 (C, phenyl), 114.0 (C, phenyl), 68.3 (CH_2, sp^3), 31.9 (CH_2, sp^3), 29.5 (CH_2, sp^3), 26.1 (CH_2, sp^3), 23.05 (CH_2, sp^3), 14.49 (CH_3, sp^3). IR (film, cm^{-1}) 2930 (C–H), 1599 (C=C).

4.4.3. *p*-PTPO6 (6c). Yield 53%, m.p. 156°C. ^{1}H NMR ($CDCl_3$) 8.63 (s, 6H, triphenyleneH), 7.26–7.22 (m, 12H, H2 and H6), 6.85–6.82 (m, 12H, H3 and H5), 3.96 (t, J=6.5 Hz, 12H, $ArOCH_2$), 1.79 (quintet, J=6.8 Hz, 12H, $ArOCH_2CH_2$), 1.49–1.40 (m, 12H, $ArOCH_2CH_2CH_2$), 1.40–1.30 (m, 24 H, $ArO(CH_2)_3CH_2CH_2$), 0.92 (t, J=6.8 Hz, 18H, $ArO(CH_2)_5$ CH_3). ^{13}C NMR ($CDCl_3$) 158.0 (C, phenyl), 139.3 (C, triphenylene), 133.8 (C, phenyl), 131.1 (C, phenyl), 128.6 (C, triphenylene), 125.3 (C, triphenylene), 114.0 (C, phenyl), 67.9 (CH_2, sp^3), 31.6 (CH_2, sp^3), 29.2 (CH_2, sp^3), 25.7 (CH_2, sp^3), 22.6 (CH_2, sp^3), 14.0 (CH_3, sp^3). IR (powder, cm^{-1}) ν_{max} 2924 (C–H), 1607 (C=C). Elemental analysis: found, C 83.9, H 8.7; calc. for $C_{90}H_{108}O_6$, C 84.1, H 8.5%.

4.5. *Preparation of CPI 'compounds'*

The compounds of **6a**, **6b** and **6c** with **1a** were prepared from solution. The solids were accurately weighed in a 1:1 molar ratio, within a tolerance of ± 0.001 g, and dissolved in DCM. After solvent evaporation, the mixture was dried for three days *in vacuo*.

4.6. *Spin-transfer NMR experiments*

Saturation transfer experiments were recorded for **6a**, in $CDCl_3$ solution and at 300 K, using a Bruker DRX 500 spectrometer. Prior to the exchange experiments longitudinal relaxation times were measured via an inversion recovery experiment, to ensure that an adequate relaxation delay was used. A saturation power of 70 dB was employed for 10 s; 64 scans were acquired at each irradiation frequency and stored in 32 k of data points. The fid's were Fourier-transformed following the application of an exponential window function using an lb=0.5 Hz. Spectra were subtracted using standard spectrometer software procedures.

Acknowledgements

We thank the EPSRC and NEDO for funding.

References

[1] O. Arikainen, N. Boden, R.J. Bushby, O.R. Lozman, J.G. Vinter, A. Wood. *Angew. Chem.*, **39**, 2333 (2000).
[2] B.R. Wegewijs, L.D.A. Siebbeles, N. Boden, R.J. Bushby, B. Movaghar, O.R. Lozman, Q. Liu, A. Pecchia, L.A. Mason. *Phys. Rev. B*, **65**, 245112 (2002).
[3] O.R. Lozman, R.J. Bushby, J.G. Vinter. *J. chem. Soc., Perkin Trans. 2*, 1446 (2001).
[4] N. Boden, R.J. Bushby, G. Cooke, O.R. Lozman, Z. Lu. *J. Am. chem. Soc.*, **123**, 7915 (2001).
[5] N. Boden, R.J. Bushby, G. Headdock, O.R. Lozman, A. Wood. *Liq. Cryst.*, **28**, 139 (2001).
[6] J.K.M. Sanders, B.K. Hunter. *Modern NMR Spectroscopy. A Guide for Chemists,* 2nd Edn, Oxford University Press, Oxford (1993).
[7] J.G. Vinter. *J. comput.-aided mol. Des.*, **8**, 653 (1994).
[8] N. Boden, R.J. Bushby, O.R. Lozman. *Mol. Cryst. liq. Cryst.*, **411**, 345 (2004).
[9] O.R. Lozman. PhD thesis, Leeds, UK (2000).
[10] B. Glusen, W. Heitz, A. Kettner, J.H. Wendorf. *Liq. Cryst.*, **20**, 627 (1996).
[11] Prof. G. Ungar, University of Sheffield, personal communication.
[12] A. Keller, J.R.S. Waring. *J. polym. Sci.*, **17**, 447 (1955).
[13] B. Wunderlich. *Macromolecular Physics,* Vol. 1, p322 *et seq*, Academic Press, New York (1973).
[14] A. Hunter, J.K.M. Sanders. *J. Am. chem. Soc.*, **119**, 5525 (1990).
[15] J.G. Vinter. *J. comput.-aided mol. Des.*, **10**, 417 (1996).
[16] T.M. Long, T.M. Swagger. *J. Amer. chem. Soc.*, **124**, 3826 (2002).
[17] J.P. Amara, T.M. Swagger. *Macromol.*, **37**, 3068 (2004).
[18] P.M. Budd, B.S. Ghanem, S. Makhseed, N.B. McKeown, K.J. Msayib, C.E. Tattershall. *Chem. Commun.*, 230 (2004).
[19] P.M. Budd, N.B. McKeown, D. Fritsch. *J. mater. Chem.*, **15**, 1977 (2005).
[20] N. Boden, R.J. Bushby, J. Clements, B. Movaghar. *J. mater. Chem.*, **9**, 2081 (1999).

Downloaded At: 16:00 25 January 2011